

# Design of Independently Tunable Dual-Band Filter with High Selectivity and Compact Size Using Multipath Propagation Concept

Yue-Peng Zhong, Yang Xiong\*, and Jian Huang

**Abstract**—A novel tunable dual-band bandpass filter (DBPF) with high selectivity and independently tunable passbands is proposed in this paper. Electric and magnetic coupling is employed in this design to create transmission zeros. The proposed tunable DBPF has the advantage of fully independent and controllable passbands due to the multipath propagation mechanism. The measured results of tunable DBPF show that the center frequency of the first passband can be shifted from 2.34 to 2.45 GHz when the bias voltage  $V_L$  increases from 3 V to 15 V, and the second passband can be tuned from 4.73 to 5.04 GHz when the bias voltage  $V_H$  varies from 6 V to 15 V. Moreover, the core circuit-size of the tunable DBPF is about  $0.293\lambda_g \times 0.067\lambda_g$ , where  $\lambda_g$  is the guided wavelength at 2.4 GHz. The proposed filter exhibits the merits of fully independent and tunable passbands, high selectivity, and compact size.

## 1. INTRODUCTION

Reconfigurable transceivers have attracted much attention in the research of modern communication systems. Tunable filters are essential components in wideband wireless communications systems due to their potential to significantly reduce system size and complexity. There are many ways to implement a tunable filter. Tunable filters implemented by micro-electromechanical systems (MEMS) have the advantage of low insertion loss and are suitable for higher frequency band [1], but they cost a lot. In addition, tunable filters based on ferrite can also bring low insertion loss [2], but the response of tuning speed is slow, and it usually occupies large circuit size. By contrast, varactor diodes have more advantages in response speed, cost, and reliability, so it is widely used in tunable filters. For multiband and multifunction wireless communication systems, tunable DBPFs are more competitive. Therefore, a lot of tunable DBPFs are proposed during the past decades [3–10]. In [3, 4], DBPFs with only one tunable passband are presented. In [5, 6], two passbands of the tunable DBPFs are affected by each other, because the odd and even-mode resonances of the presented dual-mode resonator are created dependently. In [7], an asymmetric quarter-wavelength resonator pair with shared via hole is utilized to form an independently tunable DBPF. However, it does not provide good out-of-band suppression, and there are no transmission zeros (TZs) between the two passbands. Folded open loop ring resonators and lump elements are utilized to form an independently tunable DBPF with a broadband harmonic suppression characteristic [8], but the filter suffers from high insertion loss, small tuning range, and large circuit size. Based on this structure, a tunable DBPF with wide tuning range is proposed in [9], but it still occupies large circuit dimension. By separately controlling the odd- and even-mode resonant frequencies, two independently tunable passbands can be realized in [10]. However, there is little influence between these two passbands, and its small tuning range and high insertion loss should be further improved.

In this paper, a novel tunable dual-band bandpass filter (DBPF) with high selectivity and independently tunable passbands based on multipath-embedded resonators is presented. The tunable

---

*Received 31 August 2020, Accepted 12 November 2020, Scheduled 27 December 2020*

\* Corresponding author: Yang Xiong (xiongyang0291@163.com).

The authors are with the Southwest China Institute of Electronic Technology, China.

DBPF consists of two cascaded double open-ended stub-loaded shorted-circuit resonators (DOSSRs) with a common via-hole connected along the symmetric plane of the filter. Mixed electric and magnetic coupling cancelling effect and virtual ground effect are introduced to generate multiple TZs, which results in high selectivity.

## 2. DUAL-BAND TUNABLE BPF ANALYSIS AND DESIGN

### 2.1. Basic Structure of the Tunable DBPF

Figures 1(a) and 1(b) show the configuration and coupling structure of the proposed tunable DBPF, respectively, which consists of two resonators. In Figure 1(a), four varactor diodes  $C_L$  tuned by bias voltage  $V_L$  are connected to the upper half of the resonators to tune the first passband. Similarly, four varactors  $C_H$  tuned by  $V_H$  are used for second passband controlling. The open-ended stub-loaded shorted-circuit resonators create electric coupling, and a common via-hole provides magnetic coupling. This mixed coupling generates two transmission zeros, which improves the selectivity of the filter.

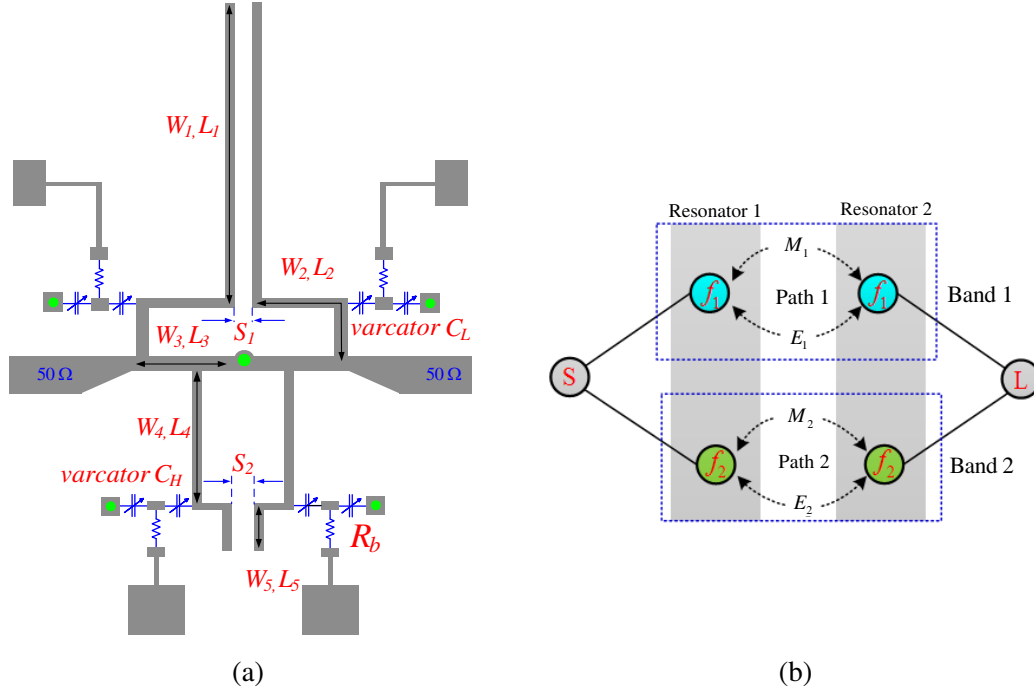


**Figure 1.** (a) Layout of the proposed tunable DBPF, (b) coupling structure.

### 2.2. Analysis of Tunable DBPF

The ideal transmission line model of the resonator is shown in Figure 2. Here,  $Y_n$  ( $n = 1, 2, L_1, L_2, H_1, H_2$ ) denotes the characteristic admittance, and  $\theta_n$  ( $n = 1, 2, L_1, L_2, H_1, H_2$ ) denotes the characteristic electrical length, respectively. The reference frequency for electrical length calculation  $f_0 = 2.4$  GHz. Then, according to the resonant condition, we let

$$\text{Im}(Y_{in}) = 0 \quad (1)$$

where  $Y_{in}$  represents the input admittance from the left side of the resonator.  $Y_H$  represents the characteristic admittance of second passband of the BPF. According to the transmission line theory, we have

$$Y_{inD} = j\omega C_H + jY_H \tan \theta_{H1} \quad (2)$$

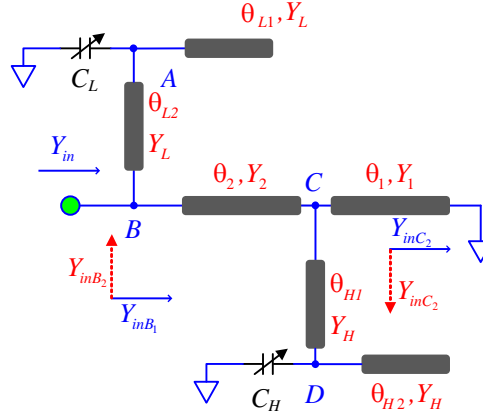


**Figure 2.** The ideal transmission line model of the DOSSR.

$$Y_{inC1} = Y_H \frac{Y_{inD} + jY_H \tan \theta_{H2}}{Y_{H2} + jY_{inD} \tan \theta_{H2}} \quad (3)$$

$$Y_{inC2} = -jY_1 \cot \theta_1 \quad (4)$$

$$Y_{inC} = Y_{inC1} + Y_{inC2} = Y_H \frac{Y_{inD} + jY_H \tan \theta_{H2}}{Y_{H2} + jY_{inD} \tan \theta_{H2}} - jY_1 \cot \theta_1 \quad (5)$$

$$Y_{inB1} = Y_2 \frac{Y_{inC} + jY_2 \tan \theta_2}{Y_2 + jY_{inC} \tan \theta_2} \quad (6)$$

$$Y_{inA} = j\omega C_L + jY_L \tan \theta_{L1} \quad (7)$$

$Y_L$  represents the characteristic admittance of first passband of the BPF.

$$Y_{inB2} = Y_L \frac{Y_{inA} + jY_L \tan \theta_{L2}}{Y_L + jY_{inA} \tan \theta_{L2}} \quad (8)$$

$$Y_{in} = Y_{inB1} + Y_{inB2} \quad (9)$$

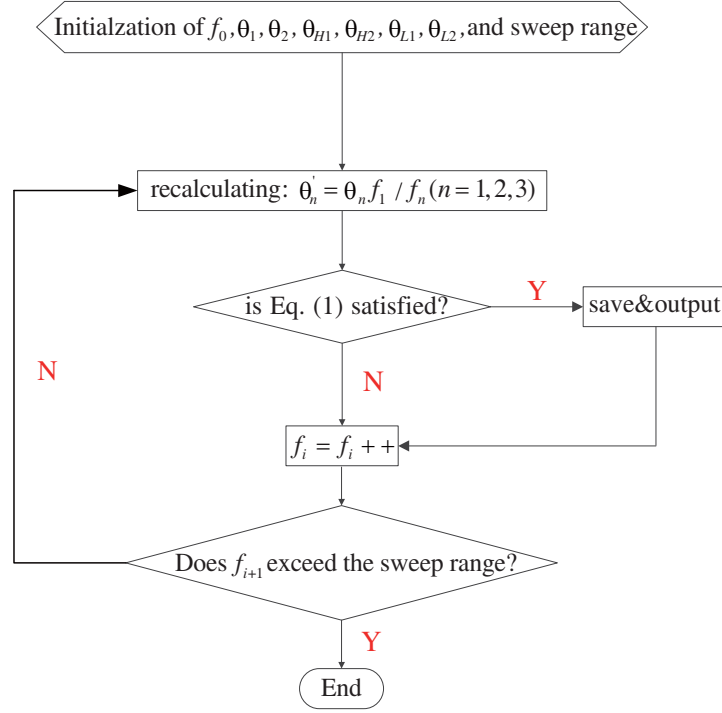
Finally, substituting Eqs. (2)~(8) into Eq. (9) we obtain:

$$Y_{in} = Y_2 \frac{Y_H \frac{j\omega C_H + jY_H \tan \theta_{H1} + jY_H \tan \theta_{H2}}{Y_{H2} + j(j\omega C_H + jY_H \tan \theta_{H1}) \tan \theta_{H2}} - jY_1 \cot \theta_1 + jY_2 \tan \theta_2}{Y_2 + j \left( Y_H \frac{j\omega C_H + jY_H \tan \theta_{H1} + jY_H \tan \theta_{H2}}{Y_{H2} + j(j\omega C_H + jY_H \tan \theta_{H1}) \tan \theta_{H2}} - jY_1 \cot \theta_1 \right) \tan \theta_2} + Y_L \frac{j\omega C_L + jY_L \tan \theta_{L1} + jY_L \tan \theta_{L2}}{Y_L + j(j\omega C_L + jY_L \tan \theta_{L1}) \tan \theta_{L2}} \quad (10)$$

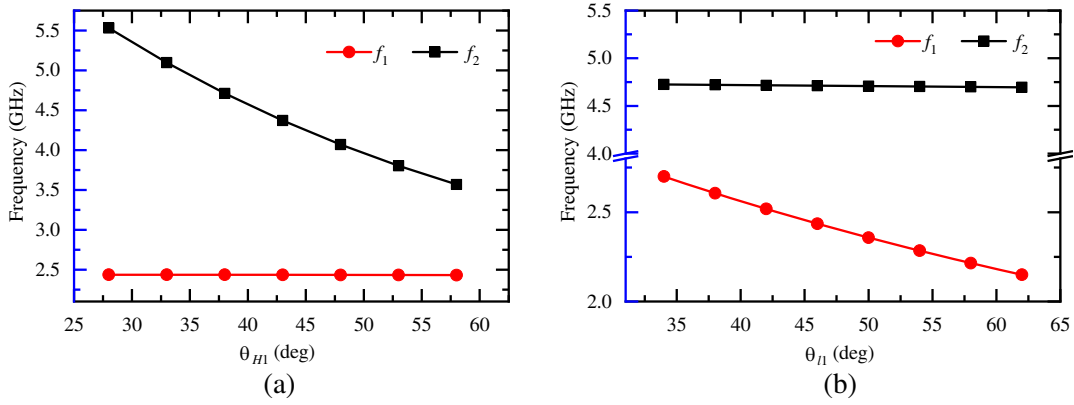
In order to observe the influence of the varactor on the resonance frequencies, MATLAB is used as a numerical calculation method to solve Eq. (1). As shown in Figure 3,  $f_1$  represents the first passband center frequency, and  $f_2$  represents the second passband center frequency.

Figure 4(a) shows that  $f_1$  keeps almost invariant when  $\theta_{H1}$  varies from  $28^\circ$  to  $58^\circ$ , while  $f_2$  shifts down dramatically. As shown in Figure 4(b), when  $\theta_H$  ( $\theta_{H1}$  and  $\theta_{H2}$ ) keeps constant, and  $\theta_{L1}$  varies from  $34^\circ$  to  $62^\circ$ , it can be found that  $f_1$  can shift down significantly, while  $f_2$  shifts down slightly. Based on these results, it can be concluded that the frequencies of the DBPF can be adjusted independently when the capacitance values of varactors are changed, as shown in Figures 5(a) and 5(b). It is noted that the frequency tuning range of the first passband is small, which is caused by the limited variation of the chosen varactors (0.03 pF–0.275 pF).

In order to clarify the multipath mechanism further, the current density distributions of the tunable DBPF are given in Figures 6(a) and 6(b), which indicates that two resonant paths are created. It is clearly observed that the first and second passbands at 2.4 and 4.9 GHz are generated by two resonant



**Figure 3.** Flow chart of solving resonant frequencies.



**Figure 4.** Resonant frequencies versus varied. (a)  $\theta_{H1}$ , (b)  $\theta_{L1}$ .

paths. It can also be found that there are no interactions between the resonators. This result is also consistent with the above calculation analysis.

Take the first passband as example. The design procedure for the tunable dual band BPF is summarized as follows:

**Step1:** According to Eq. (1), we determine the length  $L_1$ ,  $L_2$ ,  $L_3$  of the DBPF's resonator for the frequency of passband.

$$f = \frac{c}{4\sqrt{\epsilon_{re}}(L_1 + L_2 + L_3)} \quad (11)$$

where  $\epsilon_{re}$  represents the effective dielectric constant of the substrate, and  $c$  represents the speed of light in vacuum.

**Step2:** Determine the gap  $S$  of the DBPF's resonator for matching the electric coupling coefficient. The relationship between coupling coefficient and  $S$  is shown in Figure 7.

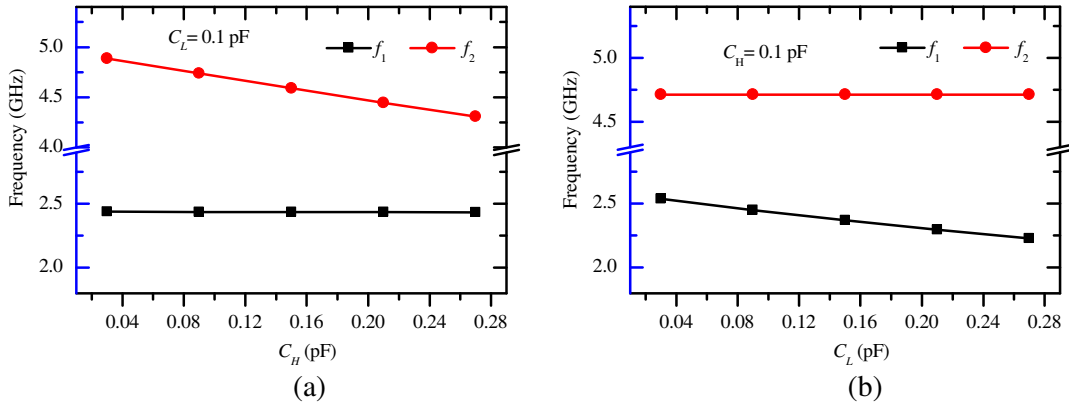


Figure 5. Resonant frequencies versus varied. (a)  $C_H$ , (b)  $C_L$ .

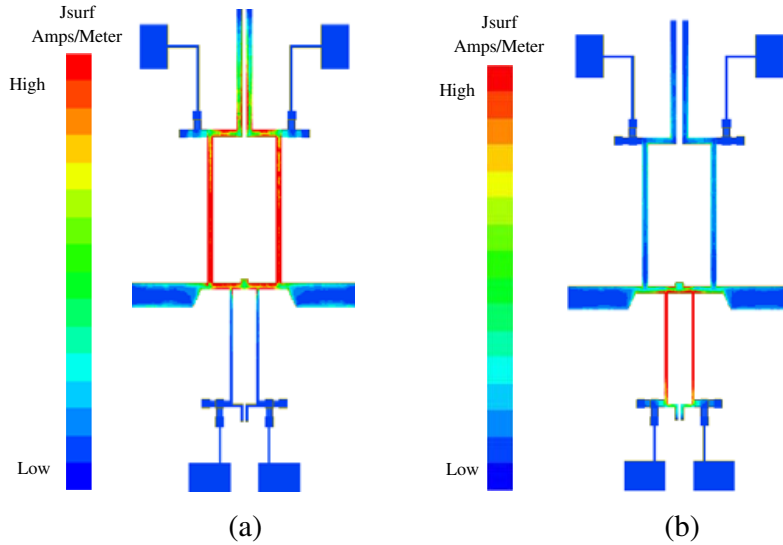


Figure 6. The dual-band BPF current density distribution. (a) @2.4 GHz, (b) @4.9 GHz.

**Step3:** Determine  $L_3$  for matching the external quality factor of the DBBPF. The relationship between external quality factor and  $L_3$  is shown in Figure 8.

Thus, physical length of the resonator can be determined according to the above analysis. The initial values of dimension parameters of the filter can be obtained according to the above analysis. The circuit parameters of dual-band BPF are as follows (unit: mm):  $L_1 = 8$ ,  $L_2 = 12.5$ ,  $L_3 = 3.15$ ,  $L_4 = 8.8$ ,  $L_5 = 5.0$ ,  $S_1 = 0.44$ ,  $S_2 = 0.205$ ,  $W_1 = W_2 = W_3 = 0.4$ ,  $W_4 = W_5 = 0.2$ . The overall size of the tunable DBPF occupies only  $27.91 \text{ mm} \times 6.36 \text{ mm}$  (excluding the feed lines), which corresponds to  $0.293\lambda_g \times 0.67\lambda_g$ , where  $\lambda_g$  is the guided wavelength at 2.4 GHz. Figures 9(a) and 9(b) depict the simulated  $S$ -parameters of the tunable DBPF.

### 3. RESULTS AND DISCUSSION

To experimentally demonstrate the tunable DBPF and verify the mentioned above numerical calculation, the tunable DBPF is fabricated on a 0.508-mm Rogers RT/Duroid 5880 substrate ( $\epsilon_r = 2.2$ ,  $\tan \delta = 0.0009$ ) with the thickness of 0.035 mm in copper etching process. Figures 10(b) and 11(b) show a photograph of the fabricated tunable DBPF where eight MAVR-011020-1411p varactor diodes ( $C_H$  &  $C_L$ ) with parasite capacitance  $C_p = 0.134 \text{ pF}$  are used to realize tunable passbands. Bias voltages

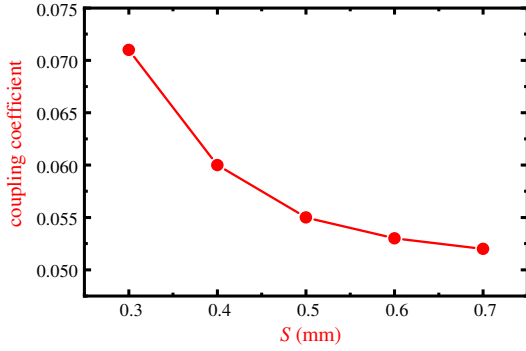


**Figure 7.** The relationship between the coupling coefficient of the resonator and the  $S$ .

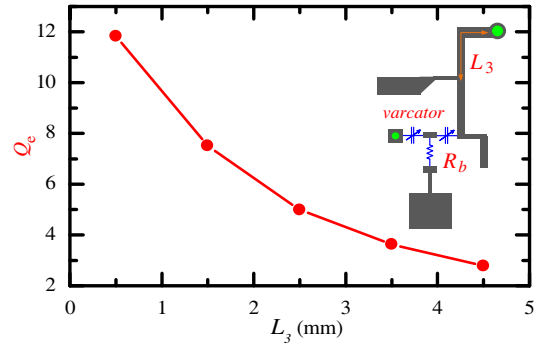


**Figure 8.** The relationship between the external quality factor of the resonator and the tapped position of  $L_3$ .

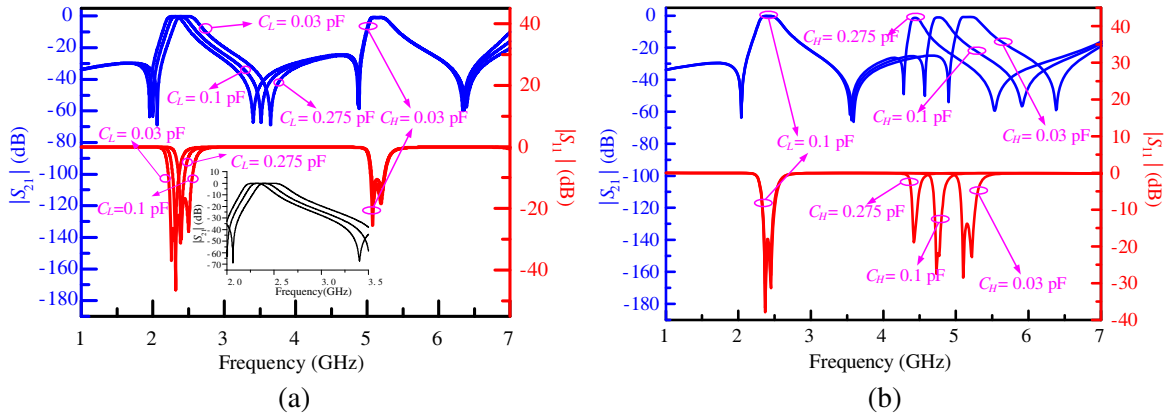


**Figure 9.** Simulated  $S$ -parameters of the proposed filter. (a) The tunable first passband with the second passband fixed, (b) the tunable second passband with the first passband fixed.

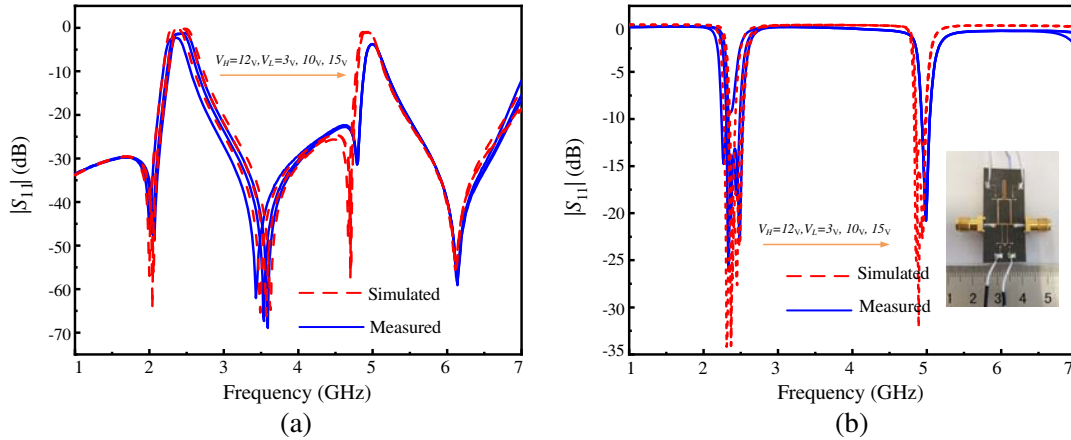


**Figure 10.** Measured and simulated results of the proposed tunable DBPF with  $V_H = 12\text{ V}$ ,  $V_L = 15\text{ V}$ ,  $10\text{ V}$ ,  $3\text{ V}$ . (a)  $|S_{21}|$ , (b)  $|S_{11}|$ .

are separately applied to the capacitors through four large resistors ( $R_b = 10\text{ k}\Omega$ ). The measured and simulated  $S$ -parameters are depicted in Figure 10 and Figure 11, respectively. As shown in Figure 10, the first passband center frequency can be tuned from 2.34 to 2.45 GHz when the second passband center frequency is fixed at 5 GHz, and the minimum insertion loss is about 1.67 dB. As can be seen, there are

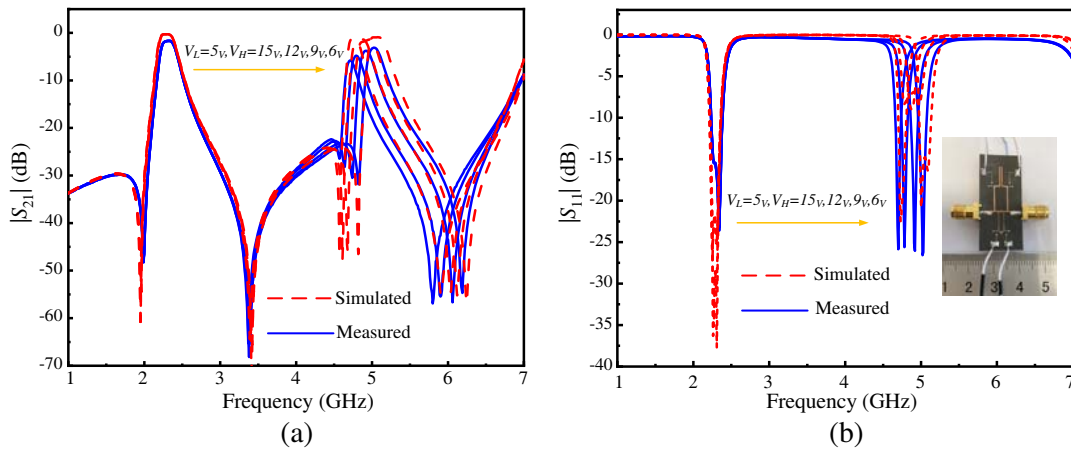


**Figure 11.** Measured and simulated results of the proposed tunable DBPF with  $V_L = 5\text{ V}$ ,  $V_H = 15\text{ V}$ , 12 V, 9 V, 6 V. (a)  $|S_{21}|$ , (b)  $|S_{11}|$ .

two TZs between the passbands, which can improve the selectivity of the filter. Figure 11 shows the measured and simulated results of the second passband. It can be found that the center frequency of the second passband is reduced from 5.04 GHz to 4.73 GHz when  $V_H$  decreases from 15 V to 0 V, while the center frequency of the first passband remains almost unchanged. The maximum band-to-band isolation can reach 70 dB.

Table 1 summarizes a comparison between this work and some reported tunable DBPFs, which shows that the proposed DBPF is of compact size, multiple TZs, and individually tunable passbands, high band-to-band isolation, etc.

**Table 1.** Comparison with some published tunable DBPFs.

Ref	Tuning range (GHz)		Insertion loss (dB)		Independently Tunable two passbands	TZs	Size ( $\lambda_g^2$ )
	$f_1$	$f_2$	$f_1$	$f_2$			
[3]	×	2.38 ~ 2.56	0.59	1.1 ~ 1.4	×	3	0.038
[4]	1.2 ~ 1.5	×	1.45 ~ 4.21	1.51	×	3	0.058
[5]	0.85 ~ 1.2	1.4 ~ 2.14	0.85 ~ 2.42	1.2 ~ 3.3	×	3	0.016
[6]	1.33 ~ 1.6	2.38 ~ 2.75	0.9 ~ 2.2	1.5 ~ 1.81	×	2	0.029
[7]	0.88 ~ 1.12	1.5 ~ 1.81	1.65 ~ 4.3	3.11 ~ 3.9	✓	0	0.033
[8]	0.88 ~ 1.08	1.68 ~ 1.85	1.4 ~ 6.9	2.3 ~ 7	✓	3	0.0893
[10]	1.25 ~ 1.36	2.1 ~ 2.31	1.46 ~ 4.3	3.1 ~ 4.85	✓	5	0.0323
This work	2.34 ~ 2.45	4.73 ~ 5.04	1.67 ~ 1.68	3.1 ~ 5.79	✓	4	0.019

#### 4. CONCLUSION

An independently tunable dual-band filter with high selectivity and compact size is presented in this paper. Electric and magnetic coupling is employed in this design to create transmission zeros. The tunable DBPF has the advantage of fully independent and controllable passbands due to the multipath propagation mechanism. The current density distributions of the filter are given to clarify the multipath mechanism. The tunable DBPF is of compact size, multiple TZs, and individually tunable passbands, which make the proposed filter attractive in multiband and multifunction wireless communication systems.

## REFERENCES

1. Zheng, A. Y., D. Psychogiou, and D. Peroulis, "Design and optimization of tunable silicon-integrated evanescent-mode bandpass filters," *IEEE Transactions on Microwave Theory and Techniques*, Vol. 66, No. 4, 1104–1113, 2018.
2. Arabi, E., F. A. Ghaffar, and A. Shamim, "Tunable bandpass filter based on partially magnetized ferrite LTCC with embedded windings for SoP applications," *IEEE Microwave and Wireless Components Letters*, Vol. 25, No. 1, 16–18, 2015.
3. Chaudhary, G. and H. Choi, "Design of dual-band bandpass filter using DGS with controllable second passband," *IEEE Microwave and Wireless Components Letters*, Vol. 21, No. 11, 589–591, 2011.
4. Zhou, L. H., Y. M. Lin, and J. Shi, "Differential dual-band bandpass filter with tunable lower band using embedded DGS unit for common-mode suppression," *IEEE Transactions on Microwave Theory and Techniques*, Vol. 64, No. 12, 32–34, 2016.
5. Chaudhary, G., Y. Jeong, and J. Lim, "Harmonic suppressed dual-band bandpass filters with tunable passbands," *IEEE Transactions on Microwave Theory and Techniques*, Vol. 60, No. 7, 2115–2123, 2012.
6. Liu, H. W., P. Wen, S. S. Zhu, and B. P. Ren, "Independently controllable dual-band microstrip bandpass filter using quadruple-mode," *International Journal of RF and Microwave Computer-aided Engineering*, Vol. 26, No. 7, 602–608, 2016.
7. Liang, F., X. Zhai, W. Lu, Q. Wang, and Y. Zhang, "An independently tunable dual-band filter using asymmetric  $\lambda/4$  resonator pairs with shared via-hole ground," *Progress In Electromagnetics Research*, Vol. 146, 99–108, 2014.
8. Feng, W. J., Y. Zhang, W. Q. Che, "Tunable dual-band filter and diplexer based on folded open loop ring resonators," *IEEE Transactions on Circuits and Systems II: Express Briefs*, Vol. 64, No. 9, 1047–1051, 2017.
9. Chen, F. C., R. S. Li, and J. P. Chen, "A tunable dual-band bandpass-to-bandstop filter using p-i-n diodes and varactors," *IEEE Access*, Vol. 6, 46058–46065, 2018.
10. Fan, Z., Y. Wang, Y. Yu, Y. Gao, Y. Zhang, Y. X. Peng, C. Guo, and J. Xu, "Compact tunable dual-band bandpass filter with independently tunable passbands and high selectivity," *IEICE Electronics Express Letter*, Vol. 16, No. 11, 1–4, 2019.